Structure
Article

Ligand-Specific Interactions Modulate Kinetic, Energetic, and Mechanical Properties of the Human β_2 Adrenergic Receptor

Michael Zocher,[1,2] Juan J. Fung,[3] Brian K. Kobilka,[3,*] and Daniel J. Müller[1,*]
[1]Department of Biosystems Science and Engineering, ETH Zürich, Mattenstr. 26, 4058 Basel, Switzerland
[2]Biozentrum, M.E. Müller Institute for Structural Biology, University of Basel, Klingelbergstr. 70, 4056 Basel, Switzerland
[3]Department of Molecular and Cellular Physiology, Stanford University School of Medicine, 279 Campus Drive, Palo Alto, CA 94305, USA
*Correspondence: kobilka@stanford.edu (B.K.K.), daniel.mueller@bsse.ethz.ch (D.J.M.)
DOI 10.1016/j.str.2012.05.010

SUMMARY

G protein-coupled receptors (GPCRs) are a class of versatile proteins that transduce signals across membranes. Extracellular stimuli induce inter- and intramolecular interactions that change the functional state of GPCRs and activate intracellular messenger molecules. How these interactions are established and how they modulate the functional state of GPCRs remain to be understood. We used dynamic single-molecule force spectroscopy to investigate how ligand binding modulates the energy landscape of the human β_2 adrenergic receptor (β_2AR). Five different ligands representing either agonists, inverse agonists or neutral antagonists established a complex network of interactions that tuned the kinetic, energetic, and mechanical properties of functionally important structural regions of β_2AR. These interactions were specific to the efficacy profile of the ligands investigated and suggest that the functional modulation of GPCRs follows structurally well-defined interaction patterns.

INTRODUCTION

G protein-coupled receptors (GPCRs) are a class of extraordinarily versatile molecules that transduce signals through cellular membranes. They respond to light, neurotransmitters, and hormones and are responsible for the senses of smell, taste, and sight. GPCRs are often described as bimodal switches that can exist in inactive and in active states. This simplified description provides only limited explanation of their complex functional behavior. For instance GPCRs can activate several G protein isoforms. Furthermore, they can trigger G protein-independent signaling pathways (Lefkowitz and Shenoy, 2005). Additionally, ligands that bind to GPCRs have distinct efficacy profiles, inducing different downstream signaling pathways. Structurally elucidating this dynamic functional behavior of GPCRs remains challenging. Recently, crystal structures of GPCRs in different functional states have been determined by Choe et al. (2011), Jaakola et al. (2008), Palczewsky et al. (2000), Rasmussen et al. (2007, 2011), Scheerer et al. (2008), Standfuss et al. (2011), and Warne et al. (2008). They suggest that binding of different ligands induces a variety of conformational and functional intermediates. In the unliganded state many GPCRs exhibit basal activity. Binding of agonists triggers a series of noncovalent intramolecular interactions, which lead to activation of the receptor. Interactions that stabilize the basal state of the receptor are disrupted, whereas interactions stabilizing active states are established (Ghanouni et al., 2001; Rosenbaum et al., 2009). Different combinations of these interactions, induced by structurally and chemically different ligands, modulate specific conformations that induce the functional intermediates involved in downstream signaling cascades.

GPCRs exhibiting a basal activity can activate their G protein even in the absence of agonists. Ligands that bind to GPCRs can either increase or decrease the basal activity, depending on their efficacy profile (Kenakin, 2002). A broad spectrum of ligands is available for GPCRs. Agonists are ligands that can activate the GPCR. Full agonists lead to maximal activation of the receptor, whereas partial agonists are not able to fully activate the GPCR, even at saturating concentrations. Inverse agonists decrease the basal activity, and neutral antagonists do not have any effect on the activity of the receptor. However, antagonists block the access of other ligands to the receptor. Depending on the ligand bound, the receptor can virtually exist in many states between fully active and fully inactive. This variety of ligand-specific conformational states explains the coexistence of multiple functional states of the receptor (Kobilka, 2011; Kobilka and Deupi, 2007).

The human β_2 adrenergic GPCR (β_2AR) is one of the most extensively studied GPCRs. Besides the α subfamily of adrenergic receptors (ARs), β_2AR belongs to the class of A receptors (Caron and Lefkowitz, 1993). Several crystal structures of β_2AR are available (Cherezov et al., 2007; Rasmussen et al., 2007, 2011; Rosenbaum et al., 2007, 2011). The β_2 receptor mainly resides in smooth muscles (Barnes, 1993), binds the hormones adrenalin and noradrenalin, and is involved in regulating cardiovascular and pulmonary function. Several ligands that bind to β_2AR are used as drugs in cardiac disease and asthma treatment (Bai, 1992). Investigating the interactions established by ligands and understanding the effect of ligand binding on the dynamic energy landscape of the receptor might help to improve the development of more efficient drugs.

Molecular interactions of membrane proteins like β_2AR can be quantified and localized by atomic force microscopy (AFM)-based single-molecule force spectroscopy (SMFS) (Kedrov

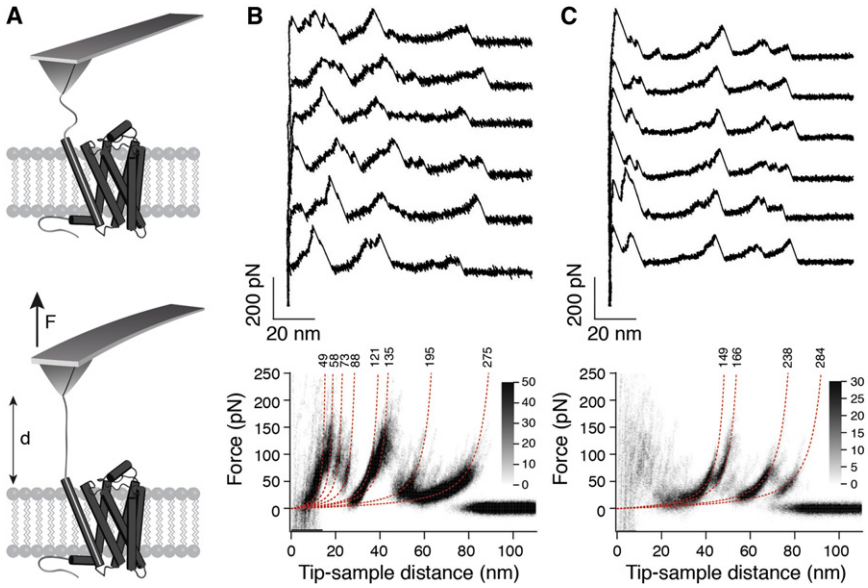

Figure 1. SMFS of β_2AR Reconstituted into Liposomes Containing Phospholipids and Cholesterol

(A) Pushing the AFM stylus onto the proteoliposomes forces the unspecific attachment of the β_2AR polypeptide to the stylus. Retraction of the cantilever stretches the polypeptide attached to the AFM stylus and induces the sequential unfolding of the receptor. F, force; d, distance.

(B and C) Selection of F-D curves recorded upon N-terminal (B, top) and C-terminal (C, top) unfolding of β_2AR. Superimpositions of 103 (B, bottom) and 56 (C, bottom) F-D curves highlight their common features. Red lines represent WLC curves fitting the main force peaks with the number on top indicating the average contour lengths (in amino acids) revealed from the fits. Gray scale bars allow evaluating how frequently individual force peaks were populated.

See also Figures S1 and S2.

et al., 2007a). Once these interactions have been assigned to secondary structure elements, parameters describing the energy landscape of the membrane protein can be determined by dynamic SMFS (DFS) (Janovjak et al., 2008). Previously, SMFS and DFS have been applied to elucidate ligand and inhibitor binding to bacterial transmembrane transporters (Bippes et al., 2009; Ge et al., 2011; Kedrov et al., 2005, 2008) and yeast mitochondrial carriers (Kedrov et al., 2010). Here, we use SMFS and DFS to determine interactions and energy barriers that are established in human β_2AR and change after binding of ligands with different efficacy profiles. To ensure native-like conditions, the receptor has been reconstituted into phospholipid liposomes containing the cholesterol analog cholesteryl hemisuccinate (CHS). Several ligands (three agonists, one inverse agonist, one neutral antagonist) were tested. Changes in energetic, kinetic, and mechanical properties of structural segments of the receptor unravel the complexity of the interaction network that determines the conformational and functional state of β_2AR.

RESULTS

Mechanical Unfolding of Human β_2AR

To determine interactions in native-like β_2AR, proteoliposomes containing β_2AR were adsorbed onto freshly cleaved mica and imaged by AFM in buffer solution (Müller and Engel, 2007). The AFM topographs showed β_2AR proteoliposomes densely covering the supporting mica (see Figure S1 available online). To nonspecifically attach single β_2AR to the AFM stylus, the stylus was pushed onto the proteoliposomes reaching a force of ~700 pN for 0.5 s (Müller and Engel, 2007). Upon withdrawal of the stylus, the receptor was mechanically stressed, and force-distance (F-D) curves were recorded (Figure 1A). Principally, β_2AR could adhere to the AFM stylus with every polypeptide loop or terminal end. Only when pulling either the N-terminal or C-terminal end and upon unfolding β_2AR into a fully stretched conformation did the F-D curves reach maximal lengths. For analysis, only F-D curves were selected, whose lengths corresponded to that of fully unfolded and stretched β_2AR polypeptides (~70–90 nm; see Experimental Procedures). About 0.5% of ~1,120,000 F-D curves showed reproducible force peak patterns that extended over the length of a fully unfolded β_2AR molecule (Figures 1B and 1C). Although the F-D curves looked similar, individual curves could differ to some extent from each other. Two major classes of F-D curves were observed (Figures 1B and 1C). To highlight common force peaks among the F-D curves, they were superimposed and converted into density plots. Each force peak of a F-D curve represents the unfolding of a structural segment of the receptor (Kedrov et al., 2007a). The magnitude of the force peak corresponds to the strength of the interaction that stabilizes a structural segment against unfolding. Such an interaction is composed of inter- and intramolecular interactions.

Unfolding β_2AR from N- and C-Terminal Ends

We assumed that the two classes of F-D curves (Figures 1B and 1C) corresponded to mechanically unfolding the receptor from the N- and C-terminal end. To assign these classes to N- or C-terminal unfolding, the N-terminal FLAG tag was enzymatically removed, and the shortened β_2AR was unfolded (Figure S2). A shift of ~14 aa was observed in one class of F-D curves, suggesting that this particular class corresponds to N-terminal unfolding. Approximately 75% of ~5,600 F-D curves corresponded to the unfolding of β_2AR by mechanically pulling the N-terminal end (Figure 1B). The remaining 25% of the F-D curves represented unfolding the receptor from the C-terminal end (Figure 1C). Superimpositions of F-D curves showed a characteristic pattern of eight force peaks when unfolding β_2AR from the N-terminal end (Figure 1B). When unfolding β_2AR from the C-terminal end, only four force peaks were detected. The C-terminal region of the receptor, which is unfolded at pulling distances <30 nm, did not reveal reproducible unfolding events (force peaks) (Figure 1C). Due to the low occurrence of C-terminally pulled F-D curves that, in addition, showed less reproducible force peaks, we focused our analysis on F-D curves pulled from the N-terminal end.

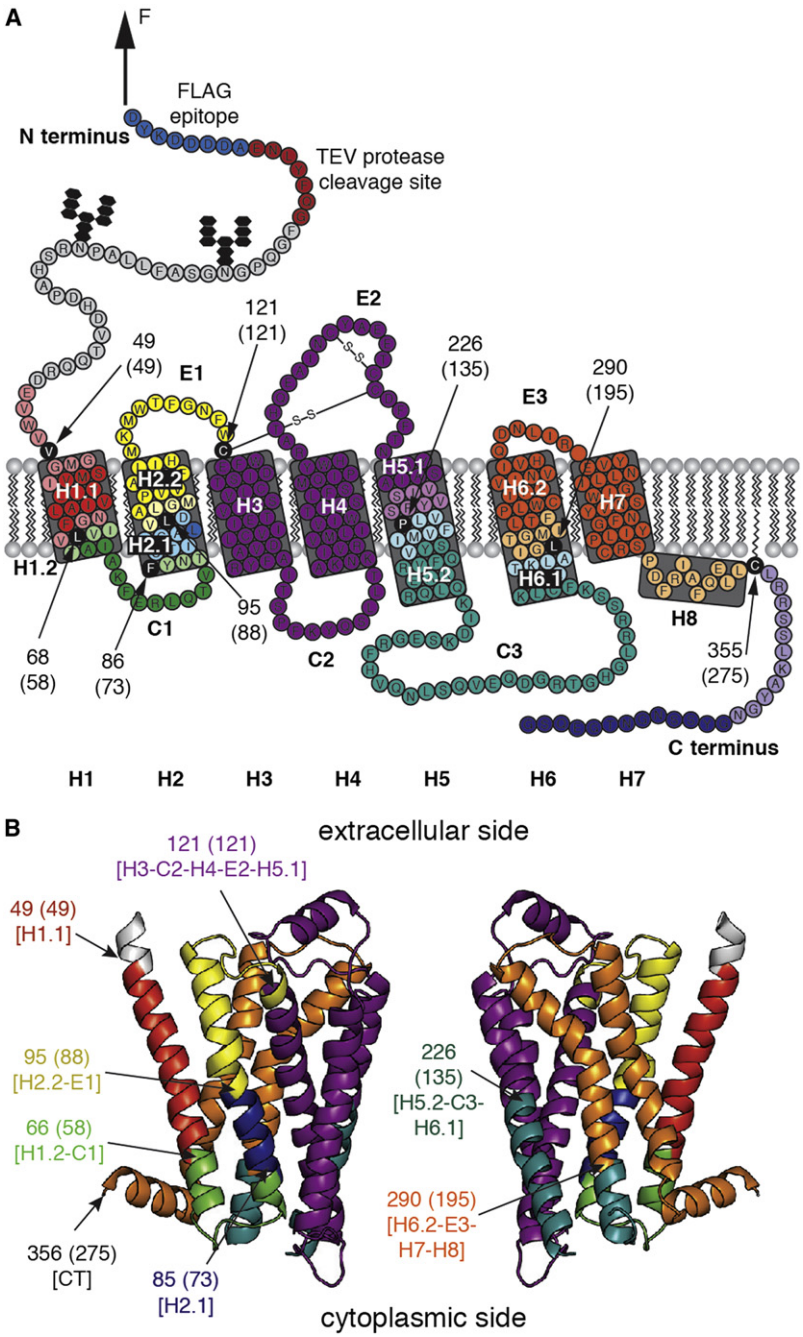

Figure 2. Structural Segments Stabilizing the Human β_2AR

Secondary (A) and tertiary (B) structure model of β_2AR is shown. Each color represents a structural segment that is stabilized by inter- and intramolecular interactions. (A) Black amino acids highlight the end of the previous and the beginning of the next stable structural segment. This structural position corresponds to the mean contour length (given in brackets) revealed from the WLC fitting of reproducibly detected force peaks in Figure 1B. Amino acids colored at less intensity give the SD of the average force peak (Table S1). In case the end/beginning of a structural segment had to be assumed to lie within the membrane or at the membrane surface opposite to the pulling AFM stylus, a certain number of amino acids were added to the contour length to structurally locate the segment (Experimental Procedures). All seven transmembrane α helices of β_2AR are labeled H1–H7. Cytoplasmic and extracellular loops are indicated as C1, C2, C3, and E1, E2, E3, respectively. H8 denotes the short C-terminal helix 8 at the cytoplasmic side. The secondary structural model (A) of C-terminal truncated β_2AR carrying a N-terminal FLAG epitope (blue) followed by a TEV protease cleavage site (green) was taken from Rasmussen et al. (2007). The tertiary structural model (B) was taken from PDB ID 2RH1. See also Figure S3 and Table S1.

Interactions Stabilize Distinct Structural Segments of β_2AR

When exerting a mechanical pulling force to a terminal end, β_2AR unfolds in sequential steps that are reflected by individual force peaks of a F-D curve (Figure 1). Every force peak was fitted using the worm-like chain (WLC) model (Experimental Procedures) to reveal the contour length of the unfolded polypeptide that connected AFM stylus and the unfolding intermediate of the receptor. The contour lengths of all force peaks allowed determining all unfolding steps of β_2AR (Figure 1; Table S1). An unfolding step, in which a structural segment unfolds, describes the transfer of one unfolding intermediate to the next (Kedrov et al., 2007a). In the first unfolding step, the N-terminal transmembrane α helix of β_2AR unfolds. After this, the polypeptide linking the AFM stylus and β_2AR is elongated and stretched again when encountering the next interaction stabilizing a structural segment of the unfolding receptor. This stepwise unfolding continues until the entire receptor unfolded. We detected eight unfolding steps, each one describing the unfolding of a structural segment stabilized by the β_2AR molecule. Mapped onto the secondary structure, these stable structural segments show where inter- and intramolecular interactions stabilized the receptor (Figure 2).

Determining Energetic, Kinetic, and Mechanical Properties Stabilizing β_2AR in the Absence and Presence of Ligands

The force required to unfold a structural segment reflects the strength of interactions stabilizing the segment. This interaction strength depends on the loading rate (pulling force applied versus time) at which the structural segment is forced to unfold (Evans, 2001). Therefore, the unfolding force gives only a relative measure of the stability of a structure exposed to mechanical stress. However, the free energy unfolding barrier describes the kinetic and mechanical stability of a folded structure at equilibrium (Figure 3A). Parameters characterizing this energy barrier can be approximated using DFS. To reveal these parameters, DFS determines the most probable interaction strengths that stabilize every structural segment over a wide range of loading rates (Evans, 2001; Janovjak et al., 2008).

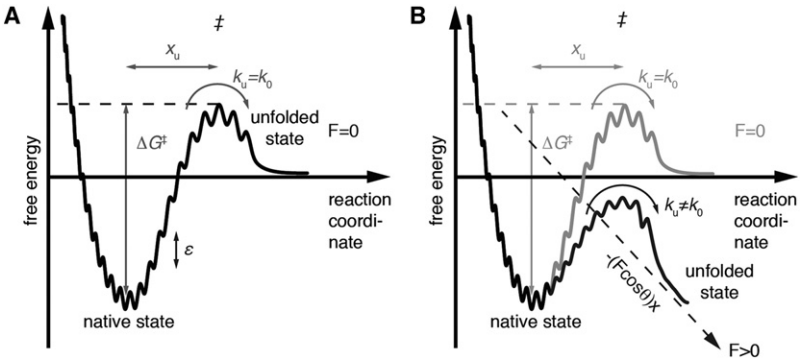

Figure 3. Free Energy Unfolding Landscape Describing Energetic and Kinetic Parameters of Stable Structural Segments

(A) According to the Bell-Evans model of Evans (1998, 2001), folded structures can be characterized using a simple two-state model. The native, folded structure resides in an energy valley and is separated by an energy barrier from the unfolded state. As approximated previously the surface roughness of the energy landscape of transmembrane α helices, ε, is ~4–6 k_BT (Janovjak et al., 2007). This roughness creates local energy minima that can stabilize functionally related conformational states of a structural segment. Thus, for a given surface roughness, a wide energy valley can host more conformational states (i.e., hosts a higher conformational variability) of a structural segment compared to a narrow energy valley. The transition state (‡) must be overcome to induce unfolding. x_u represents the distance between the folded state and the transition state, k_0 is the transition rate for crossing the energy barrier under zero force, and $\Delta G^‡$ gives the activation energy for unfolding the segment.

(B) Applying an external force (F) changes the thermal likelihood of reaching the top of the energy barrier. The energy profile along the reaction coordinate (pulling direction) is tilted by the mechanical energy -(Fcosθ)x, as indicated by the dashed line. The applied force does not change the ground-to-transition state distance x_u. θ describes the angle of the externally applied force relative to the reaction coordinate. As a result of this tilt, the energy barrier separating the folded from the unfolded state decreases, and the probability of the folded structural segment to unfold increases.

We determined the most probable unfolding force of every structural segment at different loading rates. F-D curves were recorded at seven pulling velocities (100, 300, 600, 900, 1,200, 2,500, and 5,000 nm/s) (Figure S4). To investigate to what extent the binding of different ligands affects the energy landscape of β_2AR, DFS was carried out in the unbound state and in the presence of the synthetic agonists BI-167107 (BI, Boehringer Ingelheim) and THRX-144877 (THRX, Theravance), the natural agonist adrenalin, the inverse agonist carazolol, and the neutral antagonist alprenolol. For all pulling velocities superimpositions of the F-D curves did not change drastically upon ligand binding to β_2AR (Figures S4 and S5). Next, we determined the most probable unfolding force (F^*) of every force peak characterizing a stable structural segment of β_2AR and plotted them for the different loading rates (r_f^*) (Figure 4).

Ligands Change Energy Landscape of β_2AR

As predicted by Evans (1998) and Evans and Ritchie (1997) and experimentally verified using membrane proteins by Bippes et al. (2009), Janovjak et al. (2004), Kawamura et al. (2010), Kedrov et al. (2008), Sapra et al. (2008a, 2008b), increasing the loading rate led to increased unfolding forces. The linear relationship between the most probable rupture force and the logarithm of the loading rate suggests a single energy barrier separating the folded from unfolded state for every structural segment (Evans and Ritchie, 1997). Fitting the DFS plots (Figure 4) using Equation 1 revealed the distance between ground and transition state (x_u), transition rate (k_0), free energy ($\Delta G^‡$), and mechanical spring constant (κ) of every structural segment (Figure 2). Differences between these parameters imply that the kinetic stability and mechanical nature of molecular interactions changed in the presence of ligands. To determine the statistical significance of these differences, DFS plots from ligand-free and ligand-bound β_2AR were fitted simultaneously, resulting in a common estimate for x_u and k_0. The sum of squares of both separate and simultaneous fits was assessed by an F test (Table S2) (Motulsky and Christopoulos, 2004). Several segments showed statistically significant differences after ligand binding (Table 1). In the following we will describe the significant differences detected in our experiments.

Structural Segments Changing Conformational Variability upon Ligand Binding

The distance between ground state and transition state x_u approximates the conformational variability of a structure (Figure 3) (Kumar et al., 2000). If a narrow energy valley stabilizing a structural segment becomes wider after binding of a ligand, the ligand increases the number of conformational states (i.e., conformational variability) the structural segment can adopt. Such an effect was observed upon ligand binding to β_2AR (Table 1). Binding of agonists (BI, THRX, or adrenalin) significantly increased the conformational variability of the core segment [H3-C2-H4-E2-H5.1] ($p < 0.001$), carazolol significantly increased the conformational variability of structural segments [H1.2-C1] ($p < 0.001$), [H3-C2-H4-E2-H5.1] ($p < 0.001$), and [H6.2-E3-H7-H8] ($p < 0.05$), whereas alprenolol significantly increased the conformational variability of [H1.1] ($p < 0.05$) (Table 1). These results show that ligand binding increases the conformational variability (or states) of certain structural regions of β_2AR, whereas all other structural regions were not affected significantly. It appeared that some structural regions were modulated by different ligands, whereas other regions were modulated by only one ligand. However, to what extent the conformational variability of a structural region changed was specific to the ligand.

Structural Segments Changing Lifetime upon Ligand Binding

The transition rate k_0 measures the lifetime (reciprocal of transition rate) of a structural segment. The DFS experiments (Table 1) detected that BI, THRX, or adrenalin binding significantly increased the lifetime of the structural segment [H3-C2-H4-E2-H5.1] ($p < 0.001$), that carazolol binding significantly increased the lifetime of the structural segments [H1.2-C1] ($p < 0.001$), [H2.1] ($p < 0.05$), [H3-C2-H4-E2-H5.1] ($p < 0.001$), and [H6.2-E3-H7-H8] ($p < 0.05$) and that alprenolol binding significantly

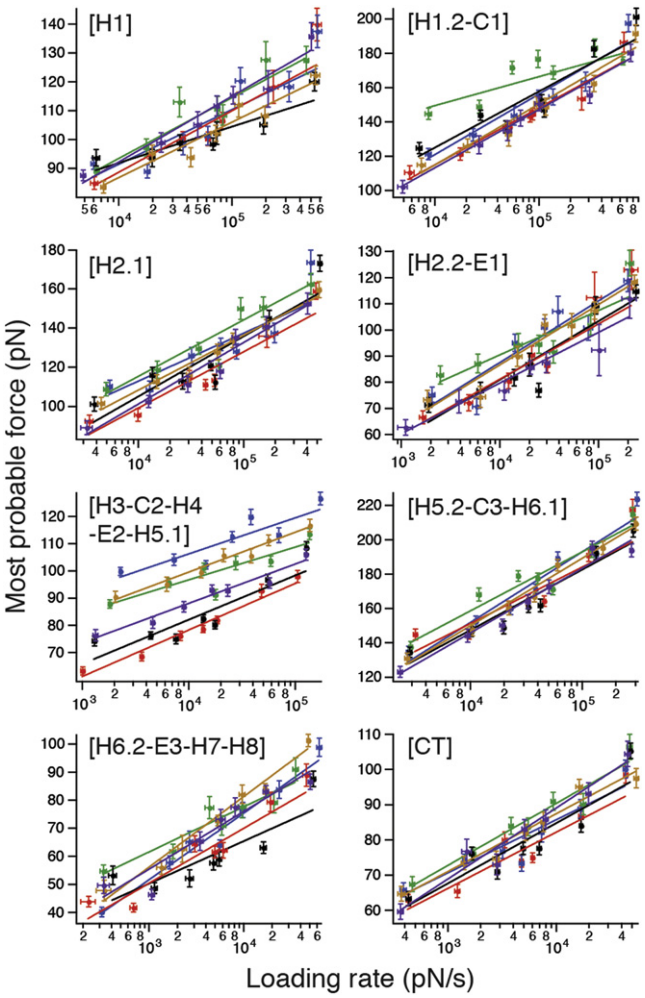

Figure 4. DFS Plots Reveal Loading Rate-Dependent Interactions Stabilizing β_2AR

For each stable structural segment of β_2AR, the most probable unfolding force was plotted against the loading rate. DFS fits using Equation 1 are shown for unliganded (red), alprenolol-bound (black), carazolol-bound (green), BI-bound (blue), THRX-bound (orange), and adrenalin-bound (violet) states. Values for x_u and k_0 obtained from fitting the DFS plots are given in Table 1. Error bars represent the SE of most probable force and loading rate. See also Figures S4 and S5.

increased the lifetime of the structural segment [H1.1] ($p < 0.05$) (Table 1). These results demonstrate that ligand binding changes the kinetic properties of structural regions within β_2AR. However, to what extent the kinetic properties of a structural region changed was again specific to the ligand.

Structural Segments Changing Free Energy upon Ligand Binding

The free energy $\Delta G^{\ddagger}$ characterizes the height of the energy barrier stabilizing a folded structure (Figure 3). DFS measurements showed that ligand binding increased the free energy of several structural segments (Table 1). BI, THRX, and adrenalin binding significantly increased $\Delta G^{\ddagger}$ of structural segment [H3-C2-H4-E2-H5.1] ($p < 0.001$), carazolol significantly increased $\Delta G^{\ddagger}$ of structural segments [H1.2-C1] ($p < 0.001$), [H2.1] ($p < 0.05$), [H3-C2-H4-E2-H5.1] ($p < 0.001$), and [H6.2-E3-H7-H8] ($p < 0.05$), and alprenolol significantly increased $\Delta G^{\ddagger}$ of structural segment [H1.1] ($p < 0.05$).

Structural Segments Changing Mechanical Properties upon Ligand Binding

Similar to the other parameters characterizing the energy barriers, the κ values that quantify the mechanical rigidity of structural segments (Dietz et al., 2006) changed upon ligand binding (Table 1). Binding of the agonists BI, THRX, and adrenalin significantly increased the mechanical elasticity of the core structural segment [H3-C2-H4-E2-H5.1] ($p < 0.001$), and alprenolol significantly decreased the mechanical elasticity of structural segment [H1.1] ($p < 0.05$). Carazolol significantly increased the mechanical elasticity of structural segments [H1.2-C1] ($p < 0.001$), [H3-C2-H4-E2-H5.1] ($p < 0.001$), and [H6.2-E3-H7-H8] ($p < 0.05$) and decreased that of structural segment [H2.1] ($p < 0.05$). These results showed that the binding of a ligand changed the mechanical properties of certain structural regions.

DISCUSSION

Ligand Binding to β_2AR Lacks Pronounced Localized Interactions

As for all membrane proteins investigated so far by SMFS (Bippes and Muller, 2011), the F-D spectra recorded during mechanical unfolding of native-like β_2AR reconstituted into proteoliposomes showed a reproducible pattern of force peaks (Figures 1B and 1C). The reproducibility of the force peak pattern suggests that β_2AR establishes a characteristic interaction network (Kedrov et al., 2007a). Ligand binding to the receptor did not establish additional force peaks or significantly modify the strength of existing force peaks (Figures S4 and S5). In contrast, SMFS detected a significantly increased force peak after ligand binding to functionally activated Na^+/H^+ antiporters NhaA from *Escherichia coli* and MjHhaP1 from *Methanococcus jannaschii* (Kedrov et al., 2005, 2007b). The increasing interaction force was correlated to specific interactions established between the ligand Na^+ and the deprotonated aspartic acid residues at the Na^+-binding site. In β_2AR multiple amino acid residues from several transmembrane α helices contribute to ligand binding (Rasmussen et al., 2011; Rosenbaum et al., 2007). Thus, it is expected that ligand binding modulates the functional state of β_2AR by changing the interaction network in the GPCR (Kobilka and Deupi, 2007). However, because we did not observe drastic changes of the force peak pattern such as observed for other membrane proteins after ligand binding (Kedrov et al., 2005, 2007b), we conclude that ligand binding established rather small changes to the interactions that structurally stabilize β_2AR in the unliganded conformation.

Conformational Variability and Kinetic Stability of Unliganded β_2AR

DFS studies suggest that structural segments of bacteriorhodopsin, bovine and mouse rhodopsin, the antiporter NhaA, and the transporter BetP are stabilized by single energy barriers (Figure 3) (Ge et al., 2011; Janovjak et al., 2004; Kawamura et al., 2010; Kedrov et al., 2008; Sapra et al., 2008c). We made

Table 1. Parameters Characterizing Energy Barriers and Mechanical Spring Constants of Structural Segments Stabilizing β_2AR

Stable Structural Segment	Unliganded β_2AR	Agonist (BI)	Agonist (THRX)	Agonist (Adrenalin)	Inverse Agonist (Carazolol)	Neutral Antagonist (Alprenolol)
	$x_u \pm$ SD (nm)					
[H1.1]	0.44 ± 0.04	0.50 ± 0.05	0.49 ± 0.07	0.47 ± 0.05	0.45 ± 0.04	0.75 ± 0.12[a]
[H1.2-C1]	0.29 ± 0.02	0.27 ± 0.02	0.30 ± 0.04	0.26 ± 0.03	0.56 ± 0.07[a]	0.29 ± 0.02
[H2.1]	0.33 ± 0.02	0.39 ± 0.04	0.39 ± 0.05	0.33 ± 0.04	0.33 ± 0.02	0.31 ± 0.02
[H2.2-E1]	0.45 ± 0.05	0.40 ± 0.04	0.40 ± 0.06	0.54 ± 0.08	0.56 ± 0.08	0.42 ± 0.03
[H3-C2-H4-E2-H5.1]	0.55 ± 0.03	0.71 ± 0.07[a]	0.73 ± 0.13[a]	0.65 ± 0.09[a]	0.79 ± 0.08[a]	0.58 ± 0.04
[H5.2-C3-H6.1]	0.29 ± 0.02	0.23 ± 0.01	0.25 ± 0.02	0.26 ± 0.02	0.28 ± 0.02	0.27 ± 0.02
[H6.2-E3-H7-H8]	0.49 ± 0.03	0.40 ± 0.02	0.39 ± 0.05	0.40 ± 0.04	0.59 ± 0.06[a]	0.58 ± 0.05
[CT]	0.59 ± 0.05	0.63 ± 0.06	0.64 ± 0.10	0.49 ± 0.06	0.54 ± 0.05	0.55 ± 0.04
	$k_0 \pm$ SD (10^{-3} s^{-1})					
[H1.1]	77.3 ± 72.5	18.7 ± 22.0	43.8 ± 64.7	26.6 ± 30.5	41.5 ± 33.9	0.09 ± 0.26[a]
[H1.2-C1]	248 ± 178	253 ± 161	121 ± 147	473 ± 372	0.002 ± 0.005[a]	111 ± 76.2
[H2.1]	290 ± 174	23.1 ± 27.1	30.5 ± 42.1	234 ± 210	80.8 ± 54.8[a]	290 ± 179
[H2.2-E1]	166 ± 140	196 ± 144	211 ± 236	38.2 ± 55.2	6.61 ± 11.5	261 ± 155
[H3-C2-H4-E2-H5.1]	38.8 ± 22.4	0.02 ± 0.03[a]	0.04 ± 0.01[a]	1.51 ± 2.75[a]	0.02 ± 0.03[a]	13.4 ± 10.4
[H5.2-C3-H6.1]	18.0 ± 13.5	118 ± 53.3	58.3 ± 41.1	59.5 ± 41.4	16.7 ± 11.5	44.5 ± 24.8
[H6.2-E3-H7-H8]	320 ± 118	663 ± 184	480 ± 300	636 ± 329	21.9 ± 20.7[a]	151 ± 106
[CT]	10.7 ± 7.98	3.28 ± 3.21	2.55 ± 4.06	33.0 ± 31.2	9.99 ± 8.90	15.4 ± 10.8
	$\Delta G^{\ddagger} \pm$ SD (k_BT)					
[H1.1]	21.0 ± 0.9	22.4 ± 1.2	21.5 ± 1.5	22.0 ± 1.1	21.6 ± 0.8	27.7 ± 2.7[a]
[H1.2-C1]	19.8 ± 0.7	19.8 ± 0.6	20.5 ± 1.2	19.2 ± 0.8	31.5 ± 2.5[a]	20.6 ± 0.7
[H2.1]	19.7 ± 0.6	22.2 ± 1.2	21.9 ± 1.4	19.9 ± 0.9	20.9 ± 0.7[a]	19.7 ± 0.6
[H2.2-E1]	20.2 ± 0.8	20.1 ± 0.7	20.0 ± 1.1	21.7 ± 1.4	23.4 ± 1.7	19.8 ± 0.6
[H3-C2-H4-E2-H5.1]	21.7 ± 0.6	29.4 ± 1.7[a]	28.6 ± 2.9[a]	24.9 ± 1.8[a]	29.3 ± 1.7[a]	22.7 ± 0.8
[H5.2-C3-H6.1]	22.4 ± 0.8	20.6 ± 0.5	21.3 ± 0.7	21.2 ± 0.7	22.5 ± 0.7	21.5 ± 0.6
[H6.2-E3-H7-H8]	19.6 ± 0.4	18.8 ± 0.3	19.2 ± 0.6	18.9 ± 0.5	22.2 ± 0.9[a]	20.3 ± 0.7
[CT]	23.0 ± 0.7	24.1 ± 1.0	24.4 ± 1.6	21.8 ± 0.9	23.0 ± 0.9	22.6 ± 0.7
	$\kappa \pm$ SD (N/m)					
[H1.1]	0.88 ± 0.13	0.74 ± 0.12	0.76 ± 0.17	0.83 ± 0.14	0.88 ± 0.12	0.40 ± 0.09[a]
[H1.2-C1]	2.02 ± 0.26	2.28 ± 0.26	1.84 ± 0.39	2.30 ± 0.40	0.83 ± 0.13[a]	2.04 ± 0.22
[H2.1]	1.49 ± 0.18	1.22 ± 0.20	1.19 ± 0.25	1.50 ± 0.27	1.60 ± 0.16[a]	1.71 ± 0.20
[H2.2-E1]	0.84 ± 0.15	1.03 ± 0.15	1.04 ± 0.25	0.61 ± 0.15	0.62 ± 0.14	0.92 ± 0.10
[H3-C2-H4-E2-H5.1]	0.59 ± 0.06	0.48 ± 0.06[a]	0.44 ± 0.11[a]	0.49 ± 0.11[a]	0.39 ± 0.05[a]	0.56 ± 0.06
[H5.2-C3-H6.1]	2.23 ± 0.25	3.21 ± 0.26	2.71 ± 0.34	2.53 ± 0.33	2.45 ± 0.24	2.47 ± 0.22
[H6.2-E3-H7-H8]	0.69 ± 0.08	0.98 ± 0.09	1.03 ± 0.20	0.99 ± 0.19	0.53 ± 0.09[a]	0.50 ± 0.08
[CT]	0.54 ± 0.06	0.51 ± 0.07	0.49 ± 0.11	0.75 ± 0.14	0.66 ± 0.09	0.61 ± 0.07

Parameters are shown for unliganded β_2AR and in the presence of two high-affinity agonists (BI and THRX), a strong partial agonist (adrenalin), an inverse agonist (carazolol), and a neutral antagonist (alprenolol). Errors represent SDs. See also Table S1.
[a]Statistically significant changes to the unliganded state as assessed by F tests (Table S2).

the same observation for the structural segments of β_2AR. The transition state distance x_u separating the folded from the unfolded state of every structural segment of β_2AR ranged from 0.3 to 0.6 nm (Table 1). Thus, the structural segments of β_2AR must be stretched by ~0.3–0.6 nm to induce unfolding. These rather short distances suggest that short-ranged inter- and intramolecular bonds, such as hydrogen bonds, van der Waals interactions, or electrostatic interactions, had to be ruptured to induce unfolding of the receptor. On average the transition state distance of structural segments determined of β_2AR was similar to the average values of ~0.4 nm determined for structural segments stabilizing bacteriorhodopsin, bovine rhodopsin, and NhaA (x_u ranging from 0.2 to 0.8 nm) (Janovjak et al., 2004; Kawamura et al., 2010; Kedrov et al., 2008; Sapra et al., 2008c). The structural segments of unliganded β_2AR revealed transition rates k_0 between 0.011 and 0.320 s^{-1} (Table 1), indicating lifetimes ranging between ~3 and ~90 s. These transition rates were in the range of those measured for other membrane proteins ranging from 0.001 to 0.9 s^{-1} (Janovjak et al., 2004; Kawamura et al., 2010; Kedrov et al., 2008; Sapra

et al., 2008c). However, the k_0 values of the structural segments of β_2AR differed by a factor of 30 with structural segments [H1.1], [H3-C2-H4-E2-H5.1], and [CT] representing the kinetically stable regions and [H1.2-C1], [H2.1], and [H6.2-E3-H7-H8] the kinetically less stable ones. Biophysical and functional studies support a multistate model of β_2AR in the absence of ligands (Deupi and Kobilka, 2010). These multiple conformational and functional states observed for unliganded β_2AR may be directly related to the conformational variability and kinetic heterogeneity of the receptor's structural segments observed by DFS.

Energetic Stability and Mechanical Elasticity of Unliganded β_2AR

The free energy barrier $\Delta G^{\ddagger}$ stabilizing the structural segments of unliganded β_2AR ranged from ~20 to 23 k_BT. These free energy differences were below that determined for structural segments of bovine rhodopsin in the inactive dark state ($\Delta G^{\ddagger}$ between 20 and 28 k_BT) (Table S3) and below those determined for the structurally similar but functionally different bacteriorhodopsin ($\Delta G^{\ddagger}$ between 21 and 29 k_BT) (Kawamura et al., 2010; Sapra et al., 2008c). Thus, the structural segments of unliganded β_2AR were energetically less stable compared to those of bovine rhodopsin and bacteriorhodopsin.

Spring constants characterizing the mechanical elasticity of structural segments in the unliganded state varied by a factor of four (Table 1). The intracellular end of α helix H1 together with the first intracellular loop [H1.2-C1] (κ = 2.02 N/m) and the structural segment [H5.2-H6.1-C3] (κ = 2.23 N/m) formed the most rigid structures of the receptor. In contrast the core segment [H3-C2-H4-E2-H5.1] (κ = 0.59 N/m) and the C-terminal domain [CT] (κ = 0.54 N/m) formed the most elastic segments. In general the structural segments stabilizing β_2AR were more elastic compared to the structural segments of bacteriorhodopsin, where the values for κ ranged from 0.9 to 4.2 N/m (Sapra et al., 2008c). Compared to the elasticity of the structural segments of bovine rhodopsin (κ between 0.16 and 2.54 N/m) (Kawamura et al., 2010), the values observed for β_2AR were more similar, indicating that both class A GPCRs share consistent mechanical properties (Table S3). However, the spring constants of the structural core segments [H3-C2-H4-E2-H5.1] of both GPCRs differed from each other. In the case of unliganded β_2AR, κ was about four times lower than κ of bovine rhodopsin in the dark state.

High Conformational Variability and Mechanical Elasticity of Structural Core Correlate to Basal β_2AR Activity

Parameters characterizing the energy barrier stabilizing unliganded β_2AR describe the receptor in its basal and low-energy state (Kobilka and Deupi, 2007). It has been suggested that the basal activity of β_2AR in the absence of ligands may be attributed to an inherent structural flexibility and tendency to adopt several conformational states (Kobilka and Deupi, 2007). In our measurements the largest segment in the receptor core [H3-C2-H4-E2-H5.1] exposed a relatively high conformational variability (high x_u) and high mechanical elasticity (low κ) compared to the other structural segments of β_2AR and compared to the core segment of the GPCR bovine rhodopsin in the dark state. This dark state of rhodopsin is stabilized by the covalently bound chromophore that acts as inverse agonist and traps the GPCRs in the inactive state (Zhukovsky and Oprian, 1989). Because the core segment of β_2AR contains multiple ligand-binding sites (Rasmussen et al., 2011; Rosenbaum et al., 2007), the increased conformational variability and mechanical elasticity allow the core to sample more conformational states required to interact with a variety of different ligands. Thus, our DFS experiments suggest that the high conformational variability and mechanical elasticity of the core segment (Table 1) contribute to the basal activity of β_2AR and favor ligand binding.

Properties of β_2AR Modified by the Neutral Antagonist Alprenolol

Neutral antagonists bind in the orthosteric pocket of a GPCR but have little or no effect on basal activity. In contrast to all other ligands tested, the neutral antagonist alprenolol only modulated the N-terminal region of transmembrane α helix H1 ([H1.1]) and widened the energy valley x_u from 0.44 nm (unliganded) to 0.75 nm. Thus, alprenolol enhanced the conformational variability of the extracellular half of α helix H1. Furthermore, binding of alprenolol significantly reduced the transition rate k_0 and increased the lifetime of structural segment [H1.1]. The free energy $\Delta G^{\ddagger}$-stabilizing structural segment [H1.1] increased by ~7 k_BT, whereas the spring constant κ decreased to 0.40 N/m (0.88 N/m in the unliganded state). These changes show that alprenolol kinetically and energetically stabilizes the extracellular part of α helix H1 and enhances its mechanical elasticity. Available crystal structures do not explain these observations. It has been suggested that α helix H1 is involved in receptor silencing by oligomerization (Guo et al., 2008; Liang et al., 2003). Therefore, it may be speculated that the alprenolol-induced kinetic and energetic stabilization as well as the structural softening of the extracellular half of α helix H1 favor oligomerization of the receptor.

Although the affinity of alprenolol (K_D ~1 nM) is comparable to that of the agonist THRX and greater than that of adrenalin, binding of the neutral antagonist did not show any effects on the structural core segment [H3-C2-H4-E2-H5.1]. Thus, alprenolol establishes very different interactions compared to THRX and to other agonists (Table 1). A possible explanation for this quite unique interaction pattern established in β_2AR could be that alprenolol has a single aromatic ring that cannot establish strong interactions with F193 of loop E2, as shown by molecular dynamics docking simulations by Bokoch et al. (2010). Moreover, in contrast to both agonists and carazolol, alprenolol does not form polar interactions with serine residues from α helix H5. This may explain that alprenolol cannot establish interactions at the core segment that are supposed to change the activity of β_2AR. In summary the DFS measurements unravel how a neutral antagonist works by simply constricting the access of other ligands to the receptor (Kenakin, 2008) and avoiding interactions at functionally important regions.

An Overall Scheme: Most Ligands Modulate the Structural Core Segment of β_2AR

To investigate to what extent ligands change the energetic, kinetic, and mechanical properties of β_2AR, we applied DFS in the presence of the synthetic agonists BI and THRX, the natural agonist adrenalin, the inverse agonist carazolol, or the neutral

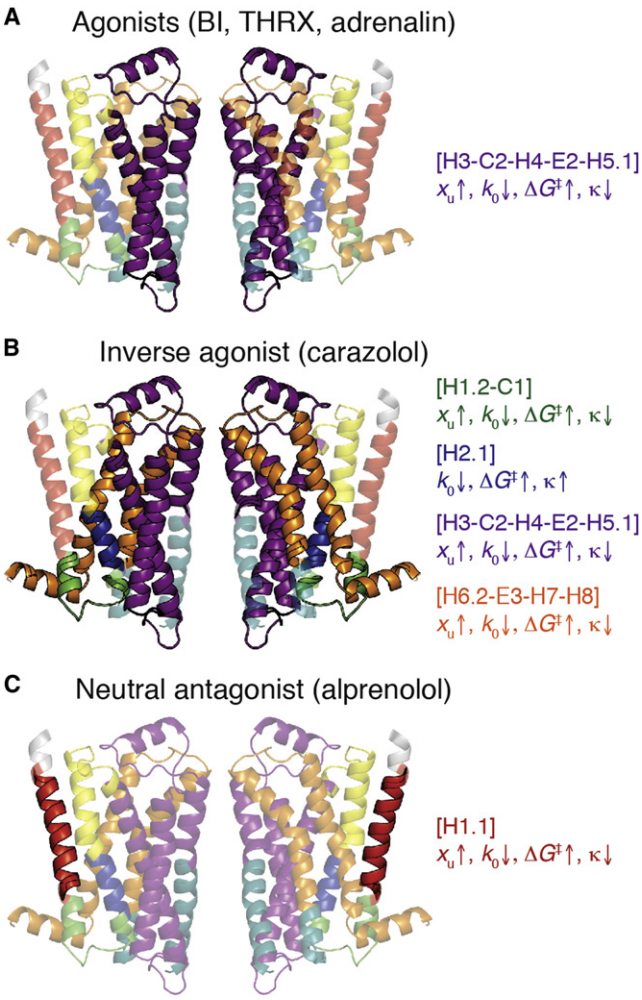

Figure 5. Structural Segments of β_2AR Changing Properties upon Ligand Binding

Structural segments that significantly change their energetic, kinetic, and mechanical properties upon binding of BI, THRX, or adrenalin (A), carazolol (B), and alprenolol (C) are highlighted (β_2AR structure PDB ID code 2RH1). Arrows denote increasing (arrow up) and decreasing (arrow down) parameters characterizing the width of the energy valley (x_u), transition rate (k_0), energy barrier ($\Delta G^{\ddagger}$), and spring constant (κ) of stable structural segments. Trends were taken from Table 1.

antagonist alprenolol. Figure 5 highlights which ligands modulate the properties of different structural segments of β_2AR. Binding of both agonists and the inverse agonist carazolol significantly modified the energetic, kinetic, and mechanical parameters of the structural core segment [H3-C2-H4-E2-H5.1]. The magnitude of the effect correlates relatively well with ligand affinity, with the lowest values being observed for the highest affinity ligands. This may be explained by extensive interactions between ligands and transmembrane α helices H3 and H5. As noted above, the small effect observed for the neutral antagonist alprenolol may be explained by the absence of polar interactions between alprenolol and transmembrane α helix H5. In the presence of agonists and carazolol, the energy valley stabilizing the structural core segment increased its distance to the transition state x_u from 0.55 nm (unliganded β_2AR) to 0.73 nm (THRX), 0.71 nm (BI), 0.65 nm (adrenalin), and 0.79 nm (carazolol). This shift toward wider energy valleys in these ligand-bound states implies that the core segment [H3-C2-H4-E2-H5.1] increases conformational variability in response to ligand binding. Furthermore, the reduction of the transition rate k_0 of the core segment by several orders of magnitude suggests that this structural region of β_2AR increases lifetime by orders of magnitude in the presence of BI, THRX, adrenalin, or carazolol. The spring constant κ of the core segment [H3-C2-H4-E2-H5.1] is slightly reduced from 0.59 N/m (unliganded state) to 0.48 N/m (BI), 0.44 N/m (THRX), 0.49 N/m (adrenalin), and 0.39 N/m (carazolol). This reduction in κ indicates that the core segment increases mechanical elasticity by ~10%–20%. Finally, ligand binding stabilized the β_2AR core segment [H3-C2-H4-E2-H5.1] by increasing free energy $\Delta G^{\ddagger}$ by 7.7 k_BT (BI), 6.9 k_BT (THRX), 3.2 k_BT (adrenalin), and 7.6 k_BT (carazolol), compared to unliganded β_2AR. Thus, the high-affinity ligands BI, THRX, and carazolol increased the free energy stabilizing the core segment twice as much compared to the natural agonist adrenalin.

Structural and functional data suggest that the core segment [H3-C2-H4-E2-H5.1] is important for ligand binding and β_2AR activation:

(1) Several amino acid residues of transmembrane α helices H3 and H5 are part of the ligand-binding pocket (Gether et al., 2002). For instance H3 and H5.1 establish polar interactions and hydrophobic contacts with BI (Rasmussen et al., 2011). Two residues of H3, D113 and V114, contribute to agonist binding (Rasmussen et al., 2011). Furthermore, S203 of H5.1 is crucial for agonist binding, as shown by mutagenesis studies by Liapakis et al. (2000).

(2) Receptor activation by agonists involves disruption of the ionic lock, which links the cytoplasmic parts of α helices H3 and H6 in the inactive state (Ballesteros et al., 2001).

(3) The second intracellular loop C2 is important for the efficiency of G protein activation and contains a switch that enables G protein coupling (Wess, 1997).

In summary DFS detected that binding of agonists and the inverse agonist carazolol increases structural flexibility, energetic stability, and lifetime (kinetic stability) of the functionally important core segment [H3-C2-H4-E2-H5.1]. These altered properties of the core segment enable β_2AR to adopt more conformations from which certain conformations are supposed to represent an active state.

The affinities of the agonists investigated range from a K_D of 0.84 pM (BI) to a K_D of 3.68 μM (adrenalin). K_D of THRX is ~1 nM. Each agonist changed the conformational variability, kinetic stability, energetic stability, and mechanical elasticity of the structural core segment [H3-C2-H4-E2-H5.1] differently. A systematic relation may be found between the kinetic stability of [H3-C2-H4-E2-H5.1], which increased with increasing affinity of the agonists that bound to β_2AR. However, it should be noted that binding of agonists alone is insufficient to stabilize β_2AR in the active state (Kobilka, 2011). Even binding of full agonists cannot stabilize every β_2AR in the active state (Yao et al., 2009). The reason for this apparent discrepancy is that although bound to a ligand, the probability of β_2ARs to adopt other

functional states lowers but does not approach zero (Kobilka and Deupi, 2007). Interestingly, the active state can be further stabilized through interactions with G proteins or camelid antibodies (nanobodies) that exhibit G protein-like behavior (Kobilka, 2011; Rasmussen et al., 2011). Characterizing such stable β_2AR/G protein complexes using DFS may be useful to quantify the conformational variability, kinetic stability, energetic stability, and mechanical elasticity of the structural core segment [H3-C2-H4-E2-H5.1] in the fully active state.

The Inverse Agonist Carazolol Introduces Major Modifications to β_2AR

Among all ligands tested, carazolol modulated the properties of most structural segments of β_2AR. Besides changing the energetic, kinetic, and mechanical properties of the core segment [H3-C2-H4-E2-H5.1] such as observed for the agonists, carazolol significantly affected three other structural segments: [H1.2-C1], [H2.1], and [H6.2-E3-H7-H8] (Table 1). Carazolol widened the energy valley stabilizing [H1.2-C1], [H3-C2-H4-E2-H5.1], and [H6.2-E3-H7-H8] by 0.10–0.27 nm. This indicates that these segments enhanced their conformational variability. Furthermore, carazolol reduced the transition rate k_0 and, thus, increased the lifetime of each of the four structural segments by up to six orders of magnitude. The free energy $\Delta G^{\ddagger}$ of structural segments [H1.2-C1] and [H3-C2-H4-E2-H5.1] increased by $\sim$10 k_BT. Carazolol slightly lowered the spring constants κ of structural segments [H2.1], [H3-C2-H4-E2-H5.1], and [H6.2-E3-H7-H8], thereby increasing their structural elasticity. The strongest effect was observed for the structural segment [H1.2-C1], where κ reduced from 2.02 N/m in the unliganded state to 0.83 N/m in the carazolol-bound state.

Several amino acid residues of α helices H3, H5, H6, and H7 are important for carazolol binding (Rosenbaum et al., 2007). For instance W109, V114, and V117 of α helix H3 establish hydrophobic contacts with carazolol. Additionally, polar interactions between carazolol and D113 of α helix H3 as well as S203 of H5.1 are crucial for carazolol binding. Furthermore, hydrophobic contacts between W286, F289, and F290 of α helix H6 and carazolol contribute to binding of the inverse agonist (Cherezov et al., 2007; Rasmussen et al., 2007). Moreover, loop E2 of the structural segment [H3-C2-H4-E2-H5.1] establishes a salt bridge with extracellular loop E3 in the inactive state (Bokoch et al., 2010). Carazolol stabilizes packing interactions involving I121 (H3), P211 (H5.1), F282 (H6.2), and N318 (H7) that contribute to a network of interactions that stabilize an inactive conformation of the receptor (Kobilka, 2011). Thus, from this point it may not be surprising that we detect that the structural segments [H3-C2-H4-E2-H5.1] and [H6.2-E3-H7-H8] change their properties upon carazolol binding. However, DFS quantifies to what extent the properties of these and other structural regions change.

Carazolol Modifies Structural Regions Proposed to Be Involved in Oligomerization

Inverse agonists promote higher-order β_2AR oligomerization that alters access to other signaling proteins (Fung et al., 2009). The significant changes of the energy barriers (x_u, k_0, and $\Delta G^{\ddagger}$) and spring constants (κ) characterizing the structural segments [H1.2-C1], [H3-C2-H4-E2-H5.1], and [H6.2-E3-H7-H8] in the presence of carazolol are of particular interest because they significantly increase conformational variability, mechanical flexibility, kinetic stability, and energetic stability upon carazolol binding. It has been proposed for several other class A GPCRs that oligomerization involves primarily the interface between α helices H1 and H8 (Guo et al., 2008; Liang et al., 2003). Thus, all structural segments changing their properties may contribute to the oligomerization of β_2AR. Particularly α helices H4 and H5 are involved in the native packing arrangement of rhodopsin and define the rhodopsin dimer (Liang et al., 2003). It is therefore likely that the increased conformational variability of the core segment [H3-C2-H4-E2-H5.1] contributes to the formation of dimers and higher-ordered oligomers in the presence of carazolol. Conversely, interactions between protomers changing their oligomeric state can influence the parameters quantified by DFS (Sapra et al., 2006a). Thus, we cannot distinguish whether changes of the structural segments are induced by carazolol binding or carazolol-induced oligomerization.

Carazolol Employs Direct and Indirect Interactions to Modify Structural Regions

Although carazolol binds to β_2AR with picomolar affinity (comparable to BI), it significantly changed the energy landscape of four structural segments. The effect of carazolol on the energy landscape of the receptor is more pronounced compared to the effects caused by any of the other agonists or the neutral antagonist investigated. Not all of the structural segments are supposed to interact directly with carazolol (Rosenbaum et al., 2007). Thus, we conclude that carazolol binding changes the properties of the structural regions of β_2AR by direct interactions and by indirect interactions, which do not result from directly contacting the ligand.

Conclusions

Energy landscapes describe conformational variability, kinetic stability, energetic stability, and mechanical elasticity of proteins (Janovjak et al., 2008). GPCRs adopt many different conformations that are closely related to functional states (Kobilka and Deupi, 2007). Our work contributes to a more detailed understanding of the energetic, kinetic, and mechanical properties of native-like β_2ARs reconstituted into membranes of phospholipids and cholesterol. We observed that the interactions of unliganded β_2AR stabilize well-defined structural segments of the receptor. In the presence of a ligand, SMFS could not detect drastic changes of these interactions, and the stabilizing structural segments did not change positions. Thus, it can be concluded that ligand binding to β_2AR induces rather weak interactions instead of strong localized interactions. However, DFS showed that the interactions established upon ligand binding were sufficient to change the conformational, energetic, kinetic, and mechanical properties of structural segments of β_2AR.

Agonist or inverse agonist binding increased the conformational variability, kinetic stability, energetic stability, and mechanical elasticity of the functionally important structural core segment [H3-C2-H4-E2-H5.1] of β_2AR. To what extent individual ligands could change the properties of the core segment was intrinsic to the ligand. In contrast to the agonists (BI, THRX, and adrenalin), the inverse agonist carazolol affected, in addition to the core segment, three structural segments: [H1.2-C1],

[H2.1], and [H6.2-E3-H7-H8]. Finally, the neutral antagonist alprenolol changed only the properties of structural segment [H1.1]. The functionally important structural core segment of the receptor remained unaffected by alprenolol.

Taken together, our single-molecule experiments reveal that ligands establish interactions that modulate the properties of distinct structural segments within β_2AR. Quantifying the energetic, kinetic, and mechanical parameters of the structural segments provides insight into how these structural segments stabilize ligand-specific conformations of the receptor. Depending on which structural segments change their energetic, kinetic, or mechanical properties, the receptor samples more active states in the presence of agonists or more inactive states in the presence of the inverse agonist.

EXPERIMENTAL PROCEDURES

Cloning, Purification, Overexpression, and Reconstitution of β_2AR

Sf9 insect cells were grown at 27°C in suspension cultures in ESF-921 medium (Expression Systems, USA) supplemented with 0.5 mg/ml gentamicin. The Bac-to-Bac Baculovirus Expression System (Invitrogen, USA) was used for generating baculovirus for the β_2AR. We used a modified construct of human β_2AR with a truncated C-terminal end (48 aa) and a N-terminal FLAG epitope followed by a TEV protease cleavage site (Figure 2). β_2AR expression was accomplished by infecting Sf9 cells at a density of ~3 × 10^6 cells/ml for ~48 hr. Cells expressing receptors, as assessed by immunofluorescence, were harvested by centrifugation (15 min at 5,000 × *g*). Cell pellets were stored at −80°C. From these pellets β_2AR was purified using a three-step purification procedure as described by Fung et al. (2009). For preparation of lipids, 1,2-dioleoyl-sn-glycero-3-phosphocholine (DOPC) (Avanti Polar Lipids, USA) and the cholesterol analog CHS (Steraloids, USA) were mixed and dissolved in chloroform to form a stock solution of lipids at concentrations of 20 and 10 mg/ml. DOPC and CHS were added to a glass vial, with DOPC at a 10-fold excess, and the chloroform was evaporated under a fine stream of argon. The lipids were then dried under vacuum for 1 hr. After this, the lipids were resuspended in 100 mM NaCl, 1% (w/v) octylclucoside, 20 mM HEPES (pH 7.5), vortexed, and sonicated for 1 hr in an ice water bath. The lipid mixture was stored at −80°C. β_2AR was reconstituted as described previously by Fung et al. (2009). Briefly, 300 μl samples were prepared containing lipid and the β_2AR at a lipid-to-receptor ratio of 1,000:1 (mol:mol). The lipid/receptor mixture was mixed with reconstitution buffer (100 mM NaCl, 20 mM HEPES [pH 7.5]) at a final volume of 300 μl and placed on ice for 2 hr. Vesicles were formed removing detergent on a Sephadex G-50 (fine) column (25 × 0.8 cm) using reconstitution buffer. To bind ligands, β_2AR was preincubated for 1 hr at room temperature (~22°C) with saturating amounts of ligand: 10 μM for BI, THRX, and carazolol, 100 μM for alprenolol, and 100 μM for adrenalin. During subsequent reconstitution steps the same concentration of ligand was included in the reconstitution buffer.

SMFS and DFS

SMFS was conducted using two different AFMs that provided similar results: ForceRobot 300 (JPK Instruments, Germany) and Nanoscope IIIa PicoForce AFM (Bruker, Germany). SMFS data of β_2AR were recorded at pulling velocities of 100, 300, 600, 900, 1,200, 2,500, and 5,000 nm/s. SMFS at pulling velocity of 5,000 nm/s was recorded using a 16 bit data acquisition hardware (Nanoscope IIIa: NI PCI-6221; ForceRobot 300: NI PCI-6251, National Instruments, Germany). Cantilevers used (60 μm long silicon nitride A-BioLever, BL-RC150 VB, Olympus, Japan) had nominal resonance frequencies of ~8 kHz in water. Cantilever spring constants (~30 pN/nm) were determined in buffer solution using the equipartition theorem by Butt and Jaschke (1995) prior to experiments. Due to uncertainties in calibrating the cantilever spring constant (~10%), β_2AR was unfolded using at least five different cantilevers for each velocity. Proteoliposomes containing β_2AR were adsorbed over night at 4°C onto freshly cleaved mica in SMFS buffer (300 mM NaCl, 25 mM $MgCl_2$, 25 mM Tris [pH 7.0]). Mica is an atomically flat, chemically inert, and hydrophilic surface that, so far, did not significantly influence the structure-function relationship of membrane proteins and their interactions probed by SMFS (Müller and Engel, 2007). To remove weakly attached membrane patches, the sample was rinsed several times with SMFS buffer. SMFS buffer solutions were prepared using nanopure water (18 MOhm/cm; PURE-LAB Ultras, ELGA LabWater) and pro-analysis grade chemicals from Sigma-Aldrich or Merck. To characterize ligand binding, SMFS buffer was supplemented with adequate amounts of the ligand. Unfolding events were monitored recording the cantilever deflection and the distance separating cantilever stylus and membrane. Interaction forces were calculated from the cantilever deflection using Hook's law.

Data Selection

Mechanical unfolding of β_2AR was recorded by F-D curves. Each force peak of a F-D curve denoted the rupture of an unfolding barrier established by a structural segment of β_2AR. The distance at which a force peak was detected assigned the contour length of the unfolded and stretched polypeptide that tethered the AFM stylus and the anchoring structural segment. The very last force peak of a F-D curve represented the unfolding of the last structural segment remaining anchored by the membrane bilayer (Müller et al., 2002). Overcoming the stability of this last segment led to complete unfolding of the receptor, followed by extraction from the membrane. In the GPCR bovine rhodopsin, the last structural segment (or unfolding barrier) corresponds to helix H8, which lies parallel to the membrane bilayer followed by a palmitoylation site (Sapra et al., 2006b). We assumed that this was also the case for β_2AR because it shares very similar structural features with rhodopsin. A fully stretched β_2AR polypeptide that remains anchored by helix H8 would show a contour length of ~260 to 290 aa. Therefore, F-D curves showing a maximum length of 70–90 nm (~260–290 aa) were selected for data analysis.

Data Analysis

Every force peak of a F-D curve was fitted using the WLC model by Bustamante et al. (1994):

$$F(x) = \frac{k_B T}{P}\left[0.25\left(1-\frac{x}{L}\right)^{-2} - 0.25 + \frac{x}{L}\right]. \quad \text{(Equation 1)}$$

A persistence length (*P*) of 0.4 nm and a backbone length of 0.36 nm were assumed for every amino acid. The contour length (*L*) (in amino acids) obtained from fitting a force peak using the WLC model describes the length of the polypeptide that had been unfolded and stretched. Contour lengths and rupture forces were statistically analyzed for every reproducibly occurring force peak using built-in and custom procedures of IgorPro 6 (WaveMetrics, USA). To superimpose F-D curves, they were aligned at the characteristic force peak detected at a contour length of 121 aa.

Assignment of Stable Structural Segments

The contour length determined by WLC fitting corresponds to the length of the unfolded and stretched β_2AR polypeptide that tethers AFM stylus and a structural unfolding intermediate. Thus, every force peak could be used to assign the end of the previous and the beginning of the following structural segment that stabilized β_2AR against unfolding (Kedrov et al., 2007a). Some stable structural segments had to be assumed to begin at the cytoplasmic β_2AR surface at the opposite side of the pulling AFM stylus. To locate the beginning of such a stable structural segment, the thickness of the membrane (~4 nm) was added to the contour length of the corresponding force peak (Kedrov et al., 2007a). Accordingly, ~11 aa (11 aa × 0.36 nm/aa) was added to the contour length of a force peak. If the beginning of a stable structural segment was located within the membrane, less amino acids were added to the contour length.

Calculation of x_u and k_0

The Bell-Evans theory by Evans (1998) describes the most probable unfolding force (F^*) as a function of the most probable loading rate (r_f^*) to reveal insight into the unfolding energy barrier that stabilizes a structural segment against unfolding (Evans and Ritchie, 1997). The relation between F^* and r_f^* can be described by:

$$F^* = \frac{k_B T}{x_u} \ln\left(\frac{x_u r_f^*}{k_B T k_0}\right). \quad \text{(Equation 2)}$$

k_B is the Boltzmann constant, T the absolute temperature, r_f^* the most probable loading rate, x_u the distance between the free energy minimum and the transition state, and k_0 the unfolding rate at zero applied force. Using a nonlinear least-squares algorithm, the parameters x_u and k_0 were obtained by fitting Equation 1 to a DFS plot (Figure 4). The loading rate was calculated using $r_f = k_{spacer}\, v$, where k_{spacer} is the spring constant of the stretched polypeptide and v the pulling velocity. k_{spacer} corresponds to the slope of a force peak before rupture. Experimental force and loading rate histograms were fitted using Gaussian distributions.

Calculation of Transition Barrier Height and Mechanical Spring Constant

The free energy barrier $\Delta G^{\ddagger}$ separating the unfolded from the folded state was calculated using the Arrhenius equation:

$$\Delta G^{\ddagger} = -k_B T \ln(\tau_D k_0). \quad \text{(Equation 3)}$$

τ_D is the diffuse relaxation time (Dietz and Rief, 2004) and is typically in a range between 10^{-7} and 10^{-9} s (Krieger et al., 2003). We used a τ_D of 10^{-8} s in our calculations. Varying τ_D in the aforementioned range would change $\Delta G^{\ddagger}$ by <15%. Furthermore, the influence of errors of τ_D would be the same for all conditions and $\Delta G^{\ddagger}$ values, even if τ_D was wrong by orders of magnitude. Errors in $\Delta G^{\ddagger}$ were calculated by propagation of errors of k_0. Without having information on the energy potential shape, we assumed a simple parabolic potential and calculated the mechanical spring constant κ of a structural segment using $\Delta G^{\ddagger}$ and x_u (Dietz et al., 2006) with the following equation:

$$\kappa = \frac{2\,\Delta G^{\ddagger}}{x_u^2}. \quad \text{(Equation 4)}$$

To estimate errors in κ, errors in $\Delta G^{\ddagger}$ and x_u were propagated.

SUPPLEMENTAL INFORMATION

Supplemental Information includes five figures and three tables and can be found with this article online at doi:10.1016/j.str.2012.05.010.

ACKNOWLEDGMENTS

Research leading to these results has received funding from the (European Community's) Seventh Framework Programme (*FP7/2007-2013*) under grant agreement No. 211800 and the DFG. We thank Ch. Bippes and K.T. Sapra for assistance and discussions.

Received: April 10, 2012
Revised: May 22, 2012
Accepted: May 22, 2012
Published online: June 28, 2012

REFERENCES

Bai, T.R. (1992). Beta 2 adrenergic receptors in asthma: a current perspective. Lung *170*, 125–141.

Ballesteros, J.A., Jensen, A.D., Liapakis, G., Rasmussen, S.G., Shi, L., Gether, U., and Javitch, J.A. (2001). Activation of the beta 2-adrenergic receptor involves disruption of an ionic lock between the cytoplasmic ends of transmembrane segments 3 and 6. J. Biol. Chem. *276*, 29171–29177.

Barnes, P.J. (1993). Beta-adrenoceptors on smooth muscle, nerves and inflammatory cells. Life Sci. *52*, 2101–2109.

Bippes, C.A., and Muller, D.J. (2011). High-resolution atomic force microscopy and spectroscopy of native membrane proteins. Rep. Prog. Phys. *74*, 086601.

Bippes, C.A., Zeltina, A., Casagrande, F., Ratera, M., Palacin, M., Muller, D.J., and Fotiadis, D. (2009). Substrate binding tunes conformational flexibility and kinetic stability of an amino acid antiporter. J. Biol. Chem. *284*, 18651–18663.

Bokoch, M.P., Zou, Y., Rasmussen, S.G., Liu, C.W., Nygaard, R., Rosenbaum, D.M., Fung, J.J., Choi, H.J., Thian, F.S., Kobilka, T.S., et al. (2010). Ligand-specific regulation of the extracellular surface of a G-protein-coupled receptor. Nature *463*, 108–112.

Bustamante, C., Marko, J.F., Siggia, E.D., and Smith, S. (1994). Entropic elasticity of lambda-phage DNA. Science *265*, 1599–1600.

Butt, H.-J., and Jaschke, M. (1995). Calculation of thermal noise in atomic-force microscopy. Nanotechnology *6*, 1–7.

Caron, M.G., and Lefkowitz, R.J. (1993). Catecholamine receptors: structure, function, and regulation. Recent Prog. Horm. Res. *48*, 277–290.

Cherezov, V., Rosenbaum, D.M., Hanson, M.A., Rasmussen, S.G., Thian, F.S., Kobilka, T.S., Choi, H.J., Kuhn, P., Weis, W.I., Kobilka, B.K., and Stevens, R.C. (2007). High-resolution crystal structure of an engineered human beta2-adrenergic G protein-coupled receptor. Science *318*, 1258–1265.

Choe, H.W., Kim, Y.J., Park, J.H., Morizumi, T., Pai, E.F., Krauss, N., Hofmann, K.P., Scheerer, P., and Ernst, O.P. (2011). Crystal structure of metarhodopsin II. Nature *471*, 651–655.

Deupi, X., and Kobilka, B.K. (2010). Energy landscapes as a tool to integrate GPCR structure, dynamics, and function. Physiology (Bethesda) *25*, 293–303.

Dietz, H., and Rief, M. (2004). Exploring the energy landscape of GFP by single-molecule mechanical experiments. Proc. Natl. Acad. Sci. USA *101*, 16192–16197.

Dietz, H., Berkemeier, F., Bertz, M., and Rief, M. (2006). Anisotropic deformation response of single protein molecules. Proc. Natl. Acad. Sci. USA *103*, 12724–12728.

Evans, E. (1998). Energy landscapes of biomolecular adhesion and receptor anchoring at interfaces explored with dynamic force spectroscopy. Faraday Discuss. *111*, 1–16.

Evans, E. (2001). Probing the relation between force—lifetime—and chemistry in single molecular bonds. Annu. Rev. Biophys. Biomol. Struct. *30*, 105–128.

Evans, E., and Ritchie, K. (1997). Dynamic strength of molecular adhesion bonds. Biophys. J. *72*, 1541–1555.

Fung, J.J., Deupi, X., Pardo, L., Yao, X.J., Velez-Ruiz, G.A., Devree, B.T., Sunahara, R.K., and Kobilka, B.K. (2009). Ligand-regulated oligomerization of beta(2)-adrenoceptors in a model lipid bilayer. EMBO J. *28*, 3315–3328.

Ge, L., Perez, C., Waclawska, I., Ziegler, C., and Muller, D.J. (2011). Locating an extracellular K+-dependent interaction site that modulates betaine-binding of the Na+-coupled betaine symporter BetP. Proc. Natl. Acad. Sci. USA *108*, E890–E898.

Gether, U., Asmar, F., Meinild, A.K., and Rasmussen, S.G. (2002). Structural basis for activation of G-protein-coupled receptors. Pharmacol. Toxicol. *91*, 304–312.

Ghanouni, P., Steenhuis, J.J., Farrens, D.L., and Kobilka, B.K. (2001). Agonist-induced conformational changes in the G-protein-coupling domain of the beta 2 adrenergic receptor. Proc. Natl. Acad. Sci. USA *98*, 5997–6002.

Guo, W., Urizar, E., Kralikova, M., Mobarec, J.C., Shi, L., Filizola, M., and Javitch, J.A. (2008). Dopamine D2 receptors form higher order oligomers at physiological expression levels. EMBO J. *27*, 2293–2304.

Jaakola, V.P., Griffith, M.T., Hanson, M.A., Cherezov, V., Chien, E.Y., Lane, J.R., Ijzerman, A.P., and Stevens, R.C. (2008). The 2.6 angstrom crystal structure of a human A2A adenosine receptor bound to an antagonist. Science *322*, 1211–1217.

Janovjak, H., Struckmeier, J., Hubain, M., Kedrov, A., Kessler, M., and Müller, D.J. (2004). Probing the energy landscape of the membrane protein bacteriorhodopsin. Structure *12*, 871–879.

Janovjak, H., Knaus, H., and Muller, D.J. (2007). Transmembrane helices have rough energy surfaces. J. Am. Chem. Soc. *129*, 246–247.

Janovjak, H., Sapra, K.T., Kedrov, A., and Müller, D.J. (2008). From valleys to ridges: exploring the dynamic energy landscape of single membrane proteins. ChemPhysChem *9*, 954–966.

Kawamura, S., Colozo, A.T., Müller, D.J., and Park, P.S. (2010). Conservation of molecular interactions stabilizing bovine and mouse rhodopsin. Biochemistry *49*, 10412–10420.

Kedrov, A., Krieg, M., Ziegler, C., Kuhlbrandt, W., and Muller, D.J. (2005). Locating ligand binding and activation of a single antiporter. EMBO Rep. *6*, 668–674.

Kedrov, A., Janovjak, H., Sapra, K.T., and Müller, D.J. (2007a). Deciphering molecular interactions of native membrane proteins by single-molecule force spectroscopy. Annu. Rev. Biophys. Biomol. Struct. *36*, 233–260.

Kedrov, A., Wegmann, S., Smits, S.H., Goswami, P., Baumann, H., and Muller, D.J. (2007b). Detecting molecular interactions that stabilize, activate and guide ligand-binding of the sodium/proton antiporter MjNhaP1 from *Methanococcus jannaschii*. J. Struct. Biol. *159*, 290–301.

Kedrov, A., Appel, M., Baumann, H., Ziegler, C., and Muller, D.J. (2008). Examining the dynamic energy landscape of an antiporter upon inhibitor binding. J. Mol. Biol. *375*, 1258–1266.

Kedrov, A., Hellawell, A.M., Klosin, A., Broadhurst, R.B., Kunji, E.R., and Müller, D.J. (2010). Probing the interactions of carboxy-atractyloside and atractyloside with the yeast mitochondrial ADP/ATP carrier. Structure *18*, 39–46.

Kenakin, T. (2002). Efficacy at G-protein-coupled receptors. Nat. Rev. Drug Discov. *1*, 103–110.

Kenakin, T.P. (2008). Pharmacological onomastics: what's in a name? Br. J. Pharmacol. *153*, 432–438.

Kobilka, B.K. (2011). Structural insights into adrenergic receptor function and pharmacology. Trends Pharmacol. Sci. *32*, 213–218.

Kobilka, B.K., and Deupi, X. (2007). Conformational complexity of G-protein-coupled receptors. Trends Pharmacol. Sci. *28*, 397–406.

Krieger, F., Fierz, B., Bieri, O., Drewello, M., and Kiefhaber, T. (2003). Dynamics of unfolded polypeptide chains as model for the earliest steps in protein folding. J. Mol. Biol. *332*, 265–274.

Kumar, S., Ma, B., Tsai, C.J., Sinha, N., and Nussinov, R. (2000). Folding and binding cascades: dynamic landscapes and population shifts. Protein Sci. *9*, 10–19.

Lefkowitz, R.J., and Shenoy, S.K. (2005). Transduction of receptor signals by beta-arrestins. Science *308*, 512–517.

Liang, Y., Fotiadis, D., Filipek, S., Saperstein, D.A., Palczewski, K., and Engel, A. (2003). Organization of the G protein-coupled receptors rhodopsin and opsin in native membranes. J. Biol. Chem. *278*, 21655–21662.

Liapakis, G., Ballesteros, J.A., Papachristou, S., Chan, W.C., Chen, X., and Javitch, J.A. (2000). The forgotten serine. A critical role for Ser-2035.42 in ligand binding to and activation of the beta 2-adrenergic receptor. J. Biol. Chem. *275*, 37779–37788.

Motulsky, H., and Christopoulos, A. (2004). Fitting Models to Biological Data Using Linear and Nonlinear Regression: A Practical Guide to Curve Fitting (New York: Oxford University Press).

Müller, D.J., and Engel, A. (2007). Atomic force microscopy and spectroscopy of native membrane proteins. Nat. Protoc. *2*, 2191–2197.

Müller, D.J., Kessler, M., Oesterhelt, F., Möller, C., Oesterhelt, D., and Gaub, H. (2002). Stability of bacteriorhodopsin alpha-helices and loops analyzed by single-molecule force spectroscopy. Biophys. J. *83*, 3578–3588.

Palczewski, K., Kumasaka, T., Hori, T., Behnke, C.A., Motoshima, H., Fox, B.A., Le Trong, I., Teller, D.C., Okada, T., Stenkamp, R.E., et al. (2000). Crystal structure of rhodopsin: A G protein-coupled receptor. Science *289*, 739–745.

Rasmussen, S.G., Choi, H.J., Rosenbaum, D.M., Kobilka, T.S., Thian, F.S., Edwards, P.C., Burghammer, M., Ratnala, V.R., Sanishvili, R., Fischetti, R.F., et al. (2007). Crystal structure of the human beta2 adrenergic G-protein-coupled receptor. Nature *450*, 383–387.

Rasmussen, S.G., Choi, H.J., Fung, J.J., Pardon, E., Casarosa, P., Chae, P.S., Devree, B.T., Rosenbaum, D.M., Thian, F.S., Kobilka, T.S., et al. (2011). Structure of a nanobody-stabilized active state of the β(2) adrenoceptor. Nature *469*, 175–180.

Rosenbaum, D.M., Cherezov, V., Hanson, M.A., Rasmussen, S.G., Thian, F.S., Kobilka, T.S., Choi, H.J., Yao, X.J., Weis, W.I., Stevens, R.C., and Kobilka, B.K. (2007). GPCR engineering yields high-resolution structural insights into beta2-adrenergic receptor function. Science *318*, 1266–1273.

Rosenbaum, D.M., Rasmussen, S.G., and Kobilka, B.K. (2009). The structure and function of G-protein-coupled receptors. Nature *459*, 356–363.

Rosenbaum, D.M., Zhang, C., Lyons, J.A., Holl, R., Aragao, D., Arlow, D.H., Rasmussen, S.G., Choi, H.J., Devree, B.T., Sunahara, R.K., et al. (2011). Structure and function of an irreversible agonist-β(2) adrenoceptor complex. Nature *469*, 236–240.

Sapra, K.T., Besir, H., Oesterhelt, D., and Muller, D.J. (2006a). Characterizing molecular interactions in different bacteriorhodopsin assemblies by single-molecule force spectroscopy. J. Mol. Biol. *355*, 640–650.

Sapra, K.T., Park, P.S.-H., Filipek, S., Engel, A., Müller, D.J., and Palczewski, K. (2006b). Detecting molecular interactions that stabilize native bovine rhodopsin. J. Mol. Biol. *358*, 255–269.

Sapra, K.T., Balasubramanian, G.P., Labudde, D., Bowie, J.U., and Muller, D.J. (2008a). Point mutations in membrane proteins reshape energy landscape and populate different unfolding pathways. J. Mol. Biol. *376*, 1076–1090.

Sapra, K.T., Doehner, J., Renugopalakrishnan, V., Padrós, E., and Muller, D.J. (2008b). Role of extracellular glutamic acids in the stability and energy landscape of bacteriorhodopsin. Biophys. J. *95*, 3407–3418.

Sapra, K.T., Park, P.S., Palczewski, K., and Muller, D.J. (2008c). Mechanical properties of bovine rhodopsin and bacteriorhodopsin: possible roles in folding and function. Langmuir *24*, 1330–1337.

Scheerer, P., Park, J.H., Hildebrand, P.W., Kim, Y.J., Krauss, N., Choe, H.W., Hofmann, K.P., and Ernst, O.P. (2008). Crystal structure of opsin in its G-protein-interacting conformation. Nature *455*, 497–502.

Standfuss, J., Edwards, P.C., D'Antona, A., Fransen, M., Xie, G., Oprian, D.D., and Schertler, G.F. (2011). The structural basis of agonist-induced activation in constitutively active rhodopsin. Nature *471*, 656–660.

Warne, T., Serrano-Vega, M.J., Baker, J.G., Moukhametzianov, R., Edwards, P.C., Henderson, R., Leslie, A.G., Tate, C.G., and Schertler, G.F. (2008). Structure of a beta1-adrenergic G-protein-coupled receptor. Nature *454*, 486–491.

Wess, J. (1997). G-protein-coupled receptors: molecular mechanisms involved in receptor activation and selectivity of G-protein recognition. FASEB J. *11*, 346–354.

Yao, X.J., Vélez Ruiz, G., Whorton, M.R., Rasmussen, S.G., DeVree, B.T., Deupi, X., Sunahara, R.K., and Kobilka, B. (2009). The effect of ligand efficacy on the formation and stability of a GPCR-G protein complex. Proc. Natl. Acad. Sci. USA *106*, 9501–9506.

Zhukovsky, E.A., and Oprian, D.D. (1989). Effect of carboxylic acid side chains on the absorption maximum of visual pigments. Science *246*, 928–930.

